Soft Matter

Accepted Manuscript

This is an *Accepted Manuscript*, which has been through the Royal Society of Chemistry peer review process and has been accepted for publication.

Accepted Manuscripts are published online shortly after acceptance, before technical editing, formatting and proof reading. Using this free service, authors can make their results available to the community, in citable form, before we publish the edited article. We will replace this *Accepted Manuscript* with the edited and formatted *Advance Article* as soon as it is available.

You can find more information about *Accepted Manuscripts* in the Information for Authors.

Please note that technical editing may introduce minor changes to the text and/or graphics, which may alter content. The journal's standard Terms & Conditions and the Ethical guidelines still apply. In no event shall the Royal Society of Chemistry be held responsible for any errors or omissions in this *Accepted Manuscript* or any consequences arising from the use of any information it contains.

ROYAL SOCIETY OF CHEMISTRY

www.rsc.org/softmatter

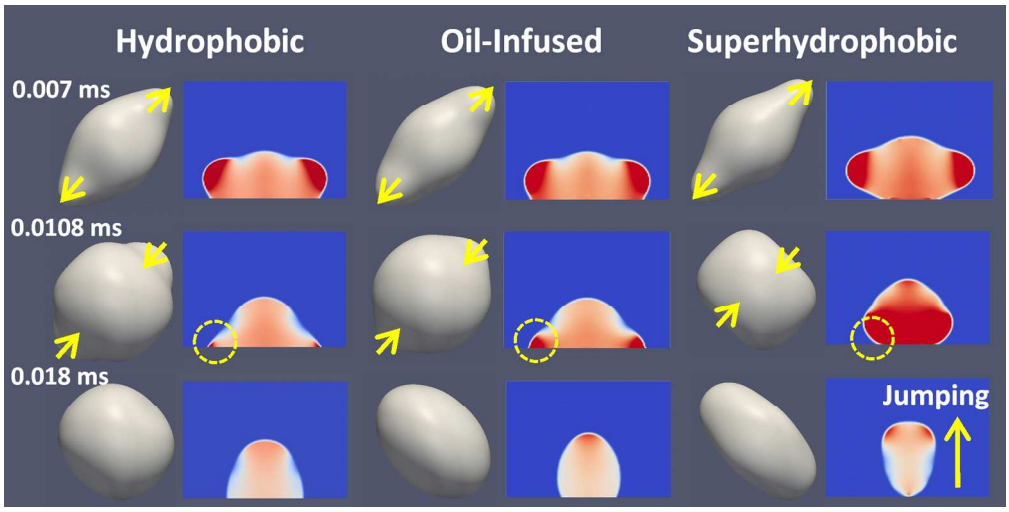

499x249mm (96 x 96 DPI)

Soft Matter Accepted Manuscript

Droplet Coalescence on Water Repellant Surfaces

Youngsuk Nam[1, a)], Donghyun Seo[1],Choongyeop Lee[2],Seungwon Shin[3, b)]

[1] Kyung Hee University, Yongin, 446-701, Korea

[2]Korea Aerospace University, Goyang, 412-791,Korea

[3]Hongik University, Seoul, 121-791, Korea

We report our hydrodynamic and energy analyses of droplet coalescence on water repellent surfaces including hydrophobic, superhydrophobic and oil-infused superhydrophobic surfaces. The receding contact angle has significant effects on the contact line dynamics since the contact line dissipation were more significant during the receding mode than advancing. The contact line dynamics are modeled by the damped harmonic oscillation equation, which shows that the damping ratio and angular frequency of merged droplets decrease as the receding contact angle increases. The fast contact line relaxation and the resulting decrease in base area during coalescence was crucial to enhance the mobility of coalescing sessile droplets by releasing more surface energy with reducing the dissipation loss. The superhydrophobic surface converts ~42% of the released surface energy to the kinetic energy via coalescence before the merged droplet jumps away from the surface, while oil-infused superhydrophobic and hydrophobic surfaces convert ~30% and ~22%, respectively, for the corresponding time. This work clarifies the mechanisms of the contact line relaxation and energy conversion during the droplet coalescence on water repellent surfaces, and helps develop water repellent condensers.

[a)]Phone: +82-31-201-3652, Electronic mail: ysnam1@khu.ac.kr

[b)]Phone: +82-2-320-3038, Electronic mail: sshin@hongik.ac.kr

Soft Matter Accepted Manuscript

The condensation on water-repellent surfaces has been actively studied to improve heat and mass transfer performances in many applications including power generation, water harvesting, and thermal management[1-5]. Previous studies have shown that the heat transfer performance of dropwisecondensation on hydrophobic surfaces is much higher than that of filmwise condensation due to the efficient gravity-driven droplet removal mechanism[6-8].Superhydrophobic condenser surfaces also haveattracted lots of attention since condensates can be spontaneously removed via the coalescence-induced jumping without any external forces such as gravity when they satisfied the energy criteria[9-12]. Recently, oil-infused superhydrophobic condenser surfaces were introduced to facilitate the condensate removal by minimizing contact line pinning and resulting hysteresis with maintaining relatively large contact area compared with superhydrophobic surfaces[13-16].

Droplet coalescence is a key process in the growth and removal of condensates, and significantly affects the overall condensation behaviors on such surfaces. However, most of the previous studies have been focused on the coalescence of freely suspended drops whose kinetics arewell described by the balance between the liquid viscosity and surface tension[17-19]. The dynamic behaviors of sessile drop coalescence are governed by complex contact line motions and energy dissipations affected by the interactions among liquid, vapor and solid phases.

When droplets merge on solid substrates, initially the liquid bridge forms between the droplets and expands. Then the merged droplet rearranges its shape from elliptical to circular[12,20,21]. Previous studies have modeled the merged droplet relaxation dynamics during the latter stage of coalescence based on the experimental observation, and defined the droplet relaxation time as t_c=

Soft Matter Accepted Manuscript

$(1/U^*)\cdot R$, where U^* represents the contact line relaxation rate and R is the final equilibrium radius[20-22]. These previous studies have found that the timescale required for the relaxation of coalescing droplets on a substrate is many orders of magnitude larger compared with that for freely suspended droplet coalescence case[20,21], which showed the significance of contact line dissipation for the sessile drop coalescence. Other previous study applied the scaling analysis and showed that the width of the growing meniscus bridge between the two droplets on highly wetting surface is proportional to $t^{1/2}$ at the early stage of coalescence[23]. These studies, however, were conducted on the substrates with moderate contact angle (40°~90°)[20-22] or highly wetting surfaces[23]and the investigations were limited on the contact line dynamics without discussing associated hydrodynamic and energy behaviors. In our recent study, we investigated the droplet coalescence on a superhydrophobic surface with a 3D model but the discussion was limited on clarifying the droplet jumping mechanism[12].

In this work, we investigated the hydrodynamic behaviors and energy conversion mechanisms of droplets coalescing on scalable hydrophobic (HPo), superhydrophobic (SHPo), oil-infused superhydrophobic (Oil-SHPo) condenser surfaces using a full 3D numerical model. We investigated the contact line dynamics during the entire coalescingevent with showing that the receding contact angle has crucial effects on contact line dynamics by affecting contact line pining and viscous dissipation. Unlike previous studies, the contact line relaxation was modeled by the damped harmonic oscillation model, which shows that both damped angular frequency and damping ratio of merged droplets decrease with increasing the receding angle.Fast contact line relaxation and resultingdecrease in the base area were found to be crucial to facilitate the

Soft Matter Accepted Manuscript

conversion from the surface energy to the kinetic energy, which explains why the droplets coalescing on SHPo and Oil-SHPo have higher mobility than the ones on HPo.

The investigated water repellent surfaces were fabricated as follows: The hydrophobic surfaces (HPo) were made by functionalizing oxygenplasma-treated commercially available copper foils with TFTS (trichloro(1H,1H,2H,2H-perfluorooctyl) silane, Sigma) through a vapor deposition process. The superhydrophobic surfaces (SHPo) were fabricated by nanostructuring the copper foils with the chemical oxidation scheme reported in our previous publications[24-26] followed by the TFTS vapor deposition. To manufacture the oil-infused superhydrophobic surfaces (Oil-SHPo), we dispensed a low viscosity oil droplet (Krytox GPL 101) on the nanostructured superhydrophobic surfaces and blew dry nitrogen gas to spread the oil uniformly on the surface[14]. Thedynamic and static contact angles measured on each investigated surface are summarized in Table 1 with the properties of the infused lubricant oil.

Detailed droplet evolution during the coalescence was investigated using a full 3D numerical model based on the level contour reconstruction method[27], a hybrid schemethat combines the advantage of the front tracking[28]and level set method[29]. Twowaterdroplets with diameter of ~30 μm are placed on the bottom of the domain and the initial shape of droplets was determined by the experimental observations on each surface.The 30 μm was selected since the droplet jumping actively occurred on the SHPo when the droplets of $d\approx$ 10~50 μm merges together in our previous experiments[12].The dynamic contact angles listed in the table 1 were incorporated to the numerical model. We use thesimpleNavier-slip model that allows thecontact line movement proportional to shear strain rateat the contact point. The contact line velocityU_{cl}isdetermined as

Soft Matter Accepted Manuscript

$U_{cl} = \lambda \cdot \partial u / \partial n|_{wall}$ where $\partial u / \partial n|_{wall}$ is the shear strain rate at the wall, and λ is proportionality constant called asaneffective slip length.

The slip length of SHPo (λ_{SHPo}) was estimated from the previous correlation $\lambda_{SHPo} = L_{eff}\left(a/\sqrt{f_s} + b\right)$[30], where $L_{eff}$is the effective pitch between the CuOnanostructures contacting liquid droplet and estimated to be 1~2 μm based on the SEM images provided in our previous studies[31]. The coefficients *a* and *b* were determined from the previous experiments (*a* = 0.325, *b* = -0.44)[30].The effective solid fraction f_s of CuO was estimated using the Cassie–Baxter equation $\cos\theta_a = f_s(\cos\theta_s + 1) - 1$. From the contact angles of the silanatedCuO (~161°) and the silanated smooth wafer (~110°),f_s was estimated to be ~0.08 andthe resulting $\lambda_{SHPo}$was~1μm. The slip length of Oil-SHPo ($\lambda_{Oil\text{-}SHPo}$) was calculated from $1/\lambda_{Oil-\mathbf{SHPo}} = 1/\{(1-f_s)\lambda_{ow}\} + 1/\lambda_{SHPo}$ [30]. The slip length between the water and the oil (Krytox GPL 101) layers was obtained from $\lambda_{ow} = (\mu_w/\mu_{oil})\delta_{oil}$, where δ_{oil} is the thickness of oil layer that was assumed to be equal to the average height of CuO nanostructures (~1 μm). The$\lambda_{ow}$was estimated to be ~33 nm and the resulting $\lambda_{Oil\text{-}SHPo}$was ~30 nm. The slip length of HPo was assumed to be zero since it was reported to be < 20 nm by previous studies[32,33].

Figure 1 shows the simulated contact line dynamics during the droplet coalescence. The evolution of the effective radius in x and y directions is defined as R_x and R_y, respectively, and extracted from the simulated results.The $R_x$and R_y were measured between the extremes of liquid-vapor interface as shown in the inset of Figure 1.The time-lapse top views and cross-sectional pressure distributions are provided in Figure 2. The simulated pressure distributions show that when the tiny liquid bridge forms between the droplets at the beginning of evolution, low

Soft Matter Accepted Manuscript

pressure field forms near the bridge due to the negative curvature of the neck. The low pressure at the neck draws a flow from the side of the droplet and thebridge expands outward. Theeffective radii R_x and R_y remain near constant at the early stage of coalescence as in Figure 1. Then R_x and R_y hit its minimum and maximum peak value at point 1 and 2, respectively, before experiencing the rapid change. At point 1 in Figures 1 and 2, the high pressure zone locates near upper center of each droplet, and then the high pressure zone circulates to the side of merged droplet at point 2. The high pressure zone requires small radius of curvatures of interface, which explains the minimum and maximum peaks at points 1 and 2, respectively.

Figure 1 also shows that there was no significant difference in contact line dynamics up to point 2 among SHPo, Oil-SHPo and HPo. Note that the contact line dynamics involves only the advancing motion up to point 2 on each surface, and therefore this feature can be explained by considering the dissipation mechanism when the contact line advances[34]. The contact line dynamics during the contact line advancing is mainly impeded by two dissipation mechanisms: the contact line pinning (*I*) and viscous dissipation (*II*). During the contact line advancing, the dissipation rate by the contact line pinning (per a unit contact line) can be approximated as $I \sim \sigma(\cos\theta_s - \cos\theta_a)U_{cl}$, and one can expect that this contribution would be negligible for all three surfaces, as advancing θ_a and static θ_s contact angles are measured to be quite close to each other (Table 1).

Meanwhile, the viscous dissipation rate inside a drop (per a unit contact line) is scaled as $II \sim \mu U_{cl}^2 R_b / h$, as long as the contact angle is sufficiently large (i.e., > 90°), with R_b and h being the base radius of the drop and the drop height, respectively. With $O(h/R_b) \sim 1$, the

Soft Matter Accepted Manuscript

viscous dissipation *II* is about μU_{cl}^2 , which indicates that the viscous dissipation rate *II* would be similar among SHPo, Oil-SHPo and HPo due to no strong dependence on the contact angle. Based on these calculations, one can conclude that there would be no significant difference in contact line dynamics among SHPo, Oil-SHP and HPo up to point 2, due to a similar amount of the overall dissipation during the contact line advancing.

Similarly with the contact line advancing, the overall dissipation mechanism is divided into two dissipation mechanisms during the contact line receding: one due to the contact line pinning ($I \sim \sigma(\cos\theta_r - \cos\theta_s)U_{cl}$) and the viscous dissipation (*II*). Only on HPo the dissipation by the contact line pinning is non-negligible due to a large difference between receding θ_r and static $\theta_s$contact angles on HPo, while its contribution remains negligible on SHPo and Oil-SHPo. Please note that when the contact angle is small and the contact line takes a wedge-like shape (as observed during the contact line receding on HPo and Oil-SHPo), the viscous dissipation would diverge near a contact line. In the small contact angle limit, the viscous dissipation rate (per a unit contact line) can be approximated as $II \sim \mu U_{cl}^2 \log(R_b / a)/\theta$ with *a* being the molecular cut-off length scale and $\log(R_b / a)$ reported to range between 15 to 20 in the previous study [35].

From the viscous dissipation in the small angle limit, it can be said that the viscous dissipation during the contact line receding is significantly larger than during the contact line advancing on HPo and Oil-SHPo due to much larger numerical coefficient involved (e.g., during receding $II \sim 20\mu U_{cl}^2/\theta \sim 20\mu U_{cl}^2$ with $\theta \sim 60°$*versus* during advancing $II \sim \mu U_{cl}^2$). Also, the viscous dissipation in the small angle limit has an explicit functional dependence on the contact angle, in a way that the smaller receding contact angle generally leads to the larger amount of dissipation

Soft Matter Accepted Manuscript

although the change in U_{cl} according to the contact angle variation also needs to be considered to make an accurate comparison. The apparent contact angle during the contact line receding becomes lower than the values reported in table 1 to compensate the viscous forceand were extracted to be ~155°, ~75° and ~50° on SHPo, Oil-SHPo and HPo, respectively, during the receding. The high apparent receding angles and resulting small effective radius of curvature creates high pressure field near the contact line, which increases the restoring force (see the dotted circles in Figure 2). Therefore the contact line relaxation rate would be the highest on SHPo, followed by Oil-SHPo and then HPo as in Figure 1.

During the sessile drop coalescence, the surface tension force is damped with the frictional forces. As the water repellency increases, the oscillation becomes more under-damped, and the Arrhenius relaxation model $R_{x,y}(t) = R_0 \exp[-(t-t_0)/t_c]$ appliedin the previous studies[20,21] does not work well for highly water repellent surfaces. In order to capture the significant oscillation shown in Figure 1, we model the droplet relaxation behavior with a damped oscillation equation $R_{x(y)} = Ae^{-\gamma t}\cos(w_d t + \phi)$, where A is the initial amplitude, γ the damping factor, ω_d the damped angular frequency, and ϕ the phase angle. Amplitude A and phase ϕ are constants determined by the initial conditions. The damped angular frequency, ω_d can be expressed as $\omega_d = \sqrt{\omega_0^2 - \gamma^2}$, where ω_0 represents the natural angular frequency.The damping ratio ζdescribing the level of damping can be calculated as $\zeta = \gamma / \omega_0$. Figure 1shows that the model well describes the contact line relaxation on water repellent surfaces, and the parameters for each best fit are provided in Table 2.

Soft Matter Accepted Manuscript

Due to the small viscous damping at the base area and the large restoring force associated with the high receding contact angle, the coalescence on SHPo becomes much more under-damped than other cases.On the investigatedSHPo, however, the oscillation on the surface was observed only for very short time since the coalesced droplet jumped away from the surfaces.Oil-SHPo has smaller damping ratio than HPo mainly due to the high restoring force associated with the high receding angle as described earlier. Both damping ratio and angular frequency decrease as the receding contact angle increases. The damping ratios of R_x and R_y on SHPo, Oil-SHPo and HPoare extracted to be 0.06, 0.160, 0.341 and 0.135, 0.312, 0.37. The damped angular frequencies of R_x and R_y on SHPo, Oil-SHPo and HPo were 0.167, 0.247, 0.284 and 0.258, 0.277, 0.343, respectively. The asymmetry in the initial shape along x and y direction is the main cause of the difference between the parameters for R_x and R_y.

The resonant frequency for inviscid single spherical drops has been derived by previous studies[36,37] and is given by the following equation: $\varpi_n = 1/2\pi \left\{(n(n-1)(n+2)\sigma)/(\rho R^3)\right\}^{1/2}$, where n is the oscillation mode. For the second mode of oscillation (n = 2) and using R = 15 μm, ρ = 998 kg/m^3 and σ = 72 mN/m for a drop radius, the water density and surface tension, one obtains the resonant frequency of 0.165 MHz, which is close to the fitted frequency (0.167 MHz) in R_x direction and comparable with the fitted frequency (0.258 MHz) in R_y direction on SHPo. Note that the Rayleigh equation analysis is applied to predict the general behavior of droplet merging qualitatively since it cannot fully capture the complexities associated with droplet merging. The difference in the fitted frequency in R_x and R_y could result from the initial asymmetry of droplet configuration, i.e., the larger R_y compared to R_x in the beginning of merging leads to the increase of the resonant frequency in R_y direction over R_x direction.

Soft Matter Accepted Manuscript

For other surfaces (Oil-SHPo, HPo), the larger difference between the calculation and the fitting parameter might be due to the stronger influence of the contact line as well as the complex dynamics of droplet merging. The influence of the contact angle of the substrate on the sessile drop has been investigated in the previous study, and it has been shown that the decrease of the contact angle leads to the increase of the resonant frequency when the contact angle ranges between 80° and 180° [38]. It agrees with the trend in the fitting frequency in the present study, which increases as the contact angle decreases.

The changes in each energy term and interfacial areas during the entirecoalescing processeswere calculated from the simulated results.The detailed information on the calculation procedures for each energy termwasdescribed in our previous publication[12] and was not repeated here. The changes in the surface energy ΔE_s, kinetic energy ΔE_k, potential energy ΔE_p and viscous dissipations ΔE_v were plotted with the changes in the liquid-vapor $\Delta A_{lv}$and liquid-solid ΔA_{ls} interfacial areas in Figures 3 and 4, respectively. All the changes are calculated based on the initial state ($\Delta E = E - E_0$ and $\Delta A = A - A_0$).

Figures 3a and 3b compare the changes in each energy term and interfacial area of droplets merging onSHPo and HPo, respectively. Figure 3a shows that the amount of the released surface energy ΔE_s during the initial stage of coalescence is similar for both SHPo and HPo, but the mechanism for the release is different. Even though the decrease in the liquid-vapor interfacial area A_{lv} of SHPo is smaller than that of HPo, the base area A_{ls} decreases on SHPowhen the coalescence starts ($\Delta A_{ls}<0$) while it increases on HPo ($\Delta A_{ls}> 0$) as in Figure 3b, which makes ΔE_s

Soft Matter Accepted Manuscript

similar on both surfaces. Note that the reduction of A_{ls}increases the amount of the released surface energy since$\Delta E_s = \sigma_{lv}\Delta A_{lv} + \sigma_{ls}\Delta A_{ls} + \sigma_{sv}\Delta A_{sv} = \sigma_{lv}(\Delta A_{lv} - \Delta A_{ls}\cos\theta)$.

When the coalescence occurs on SHPo, the liquid bridge is formed between the droplets and the interfacial stress merges the droplets together with forming a dumbbell-shaped geometry (see Figure 2). During the process, the base area (A_{ls}) of SHPo first decreases to fit the advancing contact angle. When the liquid bridges rapidly expand and hit the bottom surface, the base area increases for a short time (see the moderate peak of ΔA_{ls} of SHPo case in Figure 3b) but the high pressure field formed at the bottom makes the merged droplet jump away from the surface, which decreases the base area again.Unlike SHPo, the liquid bridge forms with contacting the surface from the very beginning of the coalescence on HPo, which causes the initial increase in the base area.

The large ΔE_s with smallA_{ls}allow SHPo to convert the surface energy to the kinetic energymore efficiently thanHPo during the coalescence. The merged droplet on SHPo jumped away from the surface without any external force around 0.018 ms (point 4). Up to this point, SHPo converts ~42 % of the released surface energy to the kinetic energy on average, while HPo convertsonly ~22 % for the corresponding time period.

The changes in each energy term and interfacial area of merging droplet on Oil-SHPo and HPo are compared in Figure 4a and 4b, respectively. On both Oil-SHPo and HPo, the base area first increasesas the liquid bridge forms with contacting the bottom surface at the beginning of coalescence, then starts to decreasewhen the contact line relaxation starts. During the contact line

Soft Matter Accepted Manuscript

receding, the base area decreases faster on Oil-SHPo than on HPo due to the higher relaxation rate of Oil-SHPo, which helps to release larger amount of surface energy compared to HPo. Up to point 4, Oil-SHPo converts ~30 % of the released surface energy to kinetic energy on average, while HPo converts ~22 %. Figures 3 and 4 show that the high contact line relaxation rate and resulting rapid decrease in the base area are crucial to facilitate the conversion from the surface energy to the kinetic energy, which explains howSHPo and Oil-SHPocan provide the enhanced mobility to the droplets via coalescence compared to HPo.

In summary, we investigated the hydrodynamic behaviors and energy conversion of droplets merging on HPo, SHPo, Oil-SHPo surfaces. The receding contact angle hadsignificant effects onthe contact line dynamics sincethe contact line pinning and viscous dissipation were more significantduring thereceding mode than advancing. The contact line relaxation was modeled with the damped harmonic oscillation equation instead of the previous Arrhenius model since the system became significantly under-damped as the receding contact angle increases. The damping ratio and angular frequency of merged droplets decreased with increasingthe receding contact angle, and the damping ratios of R_x and R_y on the invested SHPo, Oil-SHPo and HPo were found to be 0.06, 0.160, 0.341 and 0.135, 0.312, 0.37, respectively. The fast contact line relaxation and the resulting decrease in the base area helped release larger amount of surface energy with reducing dissipation loss, which provided the enhanced mobility to the coalescing sessile droplets. From the beginning of the coalescence to the jumping away from the surface, the coalescence on SHPo converts ~42 % of the leased surface energy to the kinetic energy on average, while that on Oil-SHPo and HPo convert only ~30 % and 22 % for the corresponding time period. This work clarifies the contact line relaxation and energy conversion mechanisms on

Soft Matter Accepted Manuscript

water repellent surfaces with difficult wetting characteristics, and helps develop advanced water repellent condensers.

ACKNOWLEDGMENT

This research was supported by Basic Science Research Program through the National Research Foundation of Korea (NRF) funded by the Ministry of Science, ICT & Future Planning (No. 2012R1A1A1014845) and the Ministry of Education (No. 2012R1A1A2004478).

REFERENCES

1 H. G. Andrews, E. A. Eccles, W. C. E. Schofield, and J. P. S. Badyal, Langmuir **27** (7), 3798 (2011).
2 J. M. Beér, Progress in Energy and Combustion Science **33** (2), 107 (2007).
3 A. D. Khawaji, I. K. Kutubkhanah, and J.-M. Wie, Desalination **221** (1–3), 47 (2008).
4 N. A. Patankar, Soft Matter **6** (8), 1613 (2010).
5 L. Pérez-Lombard, J. Ortiz, and C. Pout, Energy and Buildings **40** (3), 394 (2008).
6 J. W. Rose, International Journal of Heat and Mass Transfer **10** (6), 755 (1967).
7 J. W. Rose, Proceedings of the Institution of Mechanical Engineers, Part A: Journal of Power and Energy **216** (2), 115 (2002).
8 D. W. Tanner, C. J. Potter, D. Pope, and D. West, International Journal of Heat and Mass Transfer **8** (3), 419 (1965).
9 J. B. Boreyko and C.-H. Chen, Physical Review Letters **103** (18), 184501 (2009).
10 N. Miljkovic, R. Enright, Y. Nam, K. Lopez, N. Dou, J. Sack, and E. N. Wang, Nano Letters **13** (1), 179 (2012).
11 N. Miljkovic, R. Enright, and E. N. Wang, ACS Nano **6** (2), 1776 (2012).
12 Y. Nam, H. Kim, and S. Shin, Applied Physics Letters **103** (16) (2013).
13 R. Xiao, N. Miljkovic, R. Enright, and E. N. Wang, Sci. Rep. **3** (2013).
14 C. Lee, H. Kim, and Y. Nam, Langmuir**30**, 8400 (2014).
15 A. Lafuma and D. Quéré, EPL (Europhysics Letters) **96** (5), 56001 (2011).
16 T.-S. Wong, S. H. Kang, S. K. Y. Tang, E. J. Smythe, B. D. Hatton, A. Grinthal, and J. Aizenberg, Nature **477** (7365), 443 (2011).
17 J. Eggers, Physical Review Letters **80** (12), 2634 (1998).
18 V. S. Nikolayev and D. A. Beysens, Physics of Fluids **9** (11), 3227 (1997).
19 S. G. Yiantsios and R. H. Davis, Journal of Colloid and Interface Science **144** (2), 412 (1991).
20 R. Narhe, D. Beysens, and V. S. Nikolayev, Langmuir **20** (4), 1213 (2004).

Soft Matter Accepted Manuscript

[21] D. A. B. C. Andrieu, V. S. Nikolayev and Y. Pomeau Journal of Fluid Mechanics **453**, 427 (2002).
[22] V. S. Nikolayev and D. A. Beysens, Physical Review E **65** (4), 046135 (2002).
[23] W. D. Ristenpart, P. M. McCalla, R. V. Roy, and H. A. Stone, Physical Review Letters **97** (6), 064501 (2006).
[24] Y. Nam and Y. S. Ju, Journal of Adhesion Science and Technology **27**, 2163 (2013).
[25] Y. Nam, S. Sharratt, C. Byon, S.-J. Kim, and Y. S. Ju, Journal of Microelectromechanical Systems **19** (3), 581 (2010).
[26] Y. Nam, S. Sharratt, G. Cha, and Y. S. Ju, Journal of Heat Transfer **133** (10), 101502 (2011).
[27] S. Shin and D. Juric, Journal of Computational Physics **180** (2), 427 (2002).
[28] S. O. Unverdi and G. Tryggvason, Journal of Computational Physics **100** (1), 25 (1992).
[29] S. Osher and R. P. Fedkiw, Journal of Computational Physics **169** (2), 463 (2001).
[30] C. Ybert, C. Barentin, C. Cottin-Bizonne, P. Joseph, and L. Bocquet, Physics of Fluids **19** (12) (2007).
[31] R. Enright, N. Miljkovic, N. Dou, Y. Nam, and E. N. Wang, Journal of Heat Transfer **135** (9), 091304 (2013).
[32] O. I. Vinogradova and G. E. Yakubov, Langmuir **19** (4), 1227 (2003).
[33] C. Cottin-Bizonne, B. Cross, A. Steinberger, and E. Charlaix, Physical Review Letters **94** (5), 056102 (2005).
[34] F. B.-W. P.-G. de Gennes, D. Quere, *Capillarity and wetting phenomena* (Springer, New York, 2004).
[35] P. G. de Gennes, Reviews of Modern Physics **57** (3), 827 (1985).
[36] P. Brunet and J. H. Snoeijer, Eur. Phys. J. Spec. Top. **192** (1), 207 (2011).
[37] H. Lamb, *Hydrodynamics*. (Cambridge University Press, Cambridge, 1975).
[38] J. S. Sharp, D. J. Farmer, and J. Kelly, Langmuir **27** (15), 9367 (2011).

Soft Matter Accepted Manuscript

Table 1: Measured contact angles on the investigated samples

Sample	Advancing angle θ_a(º)	Receding angle θ_r(º)	Static angle θ_s(º)
SHPo (Silanated CuO)	165.1 ± 1.6	159.8 ± 3.3	161.2 ± 1.6
Oil-SHPo* (Oil-infused silanated CuO)	119.2 ± 1.4	117.5 ± 1.1	118.2 ± 1.1
HPo (Silanated Cu)	122.7 ± 1.3	81.2 ± 1.8	116.6 ± 2.4

* Infused oil:Krytox GPL 101 (ρ = 1870 kg/m^3, σ = 17.0 mN/m, $\nu = 16\times10^{-6}$ m^2/s, at 20°C)

Soft Matter Accepted Manuscript

Table 2: Extracted parameters from the best fit for each case

		ω_d (MHz)	γ (μs^{-1})	ζ	A (μm)	ϕ (rad)
R_x	**SHPo**	0.167	0.010	0.060	9.146	4.105
	Oil-SHPo	0.247	0.040	0.160	6.038	-2.632
	HPo	0.284	0.103	0.341	8.969	-2.798
R_y	**SHPo**	0.258	0.035	0.135	19.564	0.569
	Oil-SHPo	0.277	0.091	0.312	23.549	-0.618
	HPo	0.343	0.137	0.371	30.584	-1.653

Soft Matter Accepted Manuscript

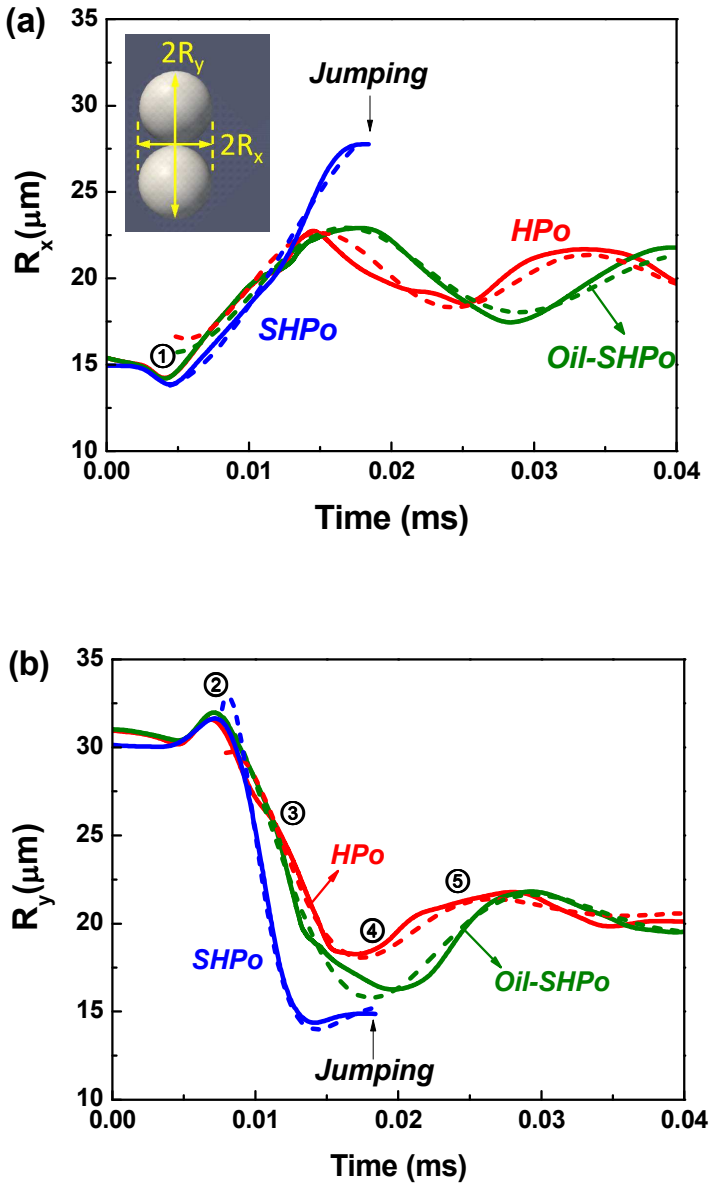

Figure 1: The evolution of a large effective radius R_x (a) and a small effective radius R_y (b), the solid lines show the results extracted from the simulation and the dotted lines show the best fits obtained from the damped harmonic oscillation equation with the parameters provided in table 2. R_x and R_y were measured between the extremes of liquid-vapor interface as in the inset of Figure 1. Points 1-5 represent t = 0.004, 0.007, 0.0108, 0.018, 0.024 (ms), respectively.

Soft Matter Accepted Manuscript

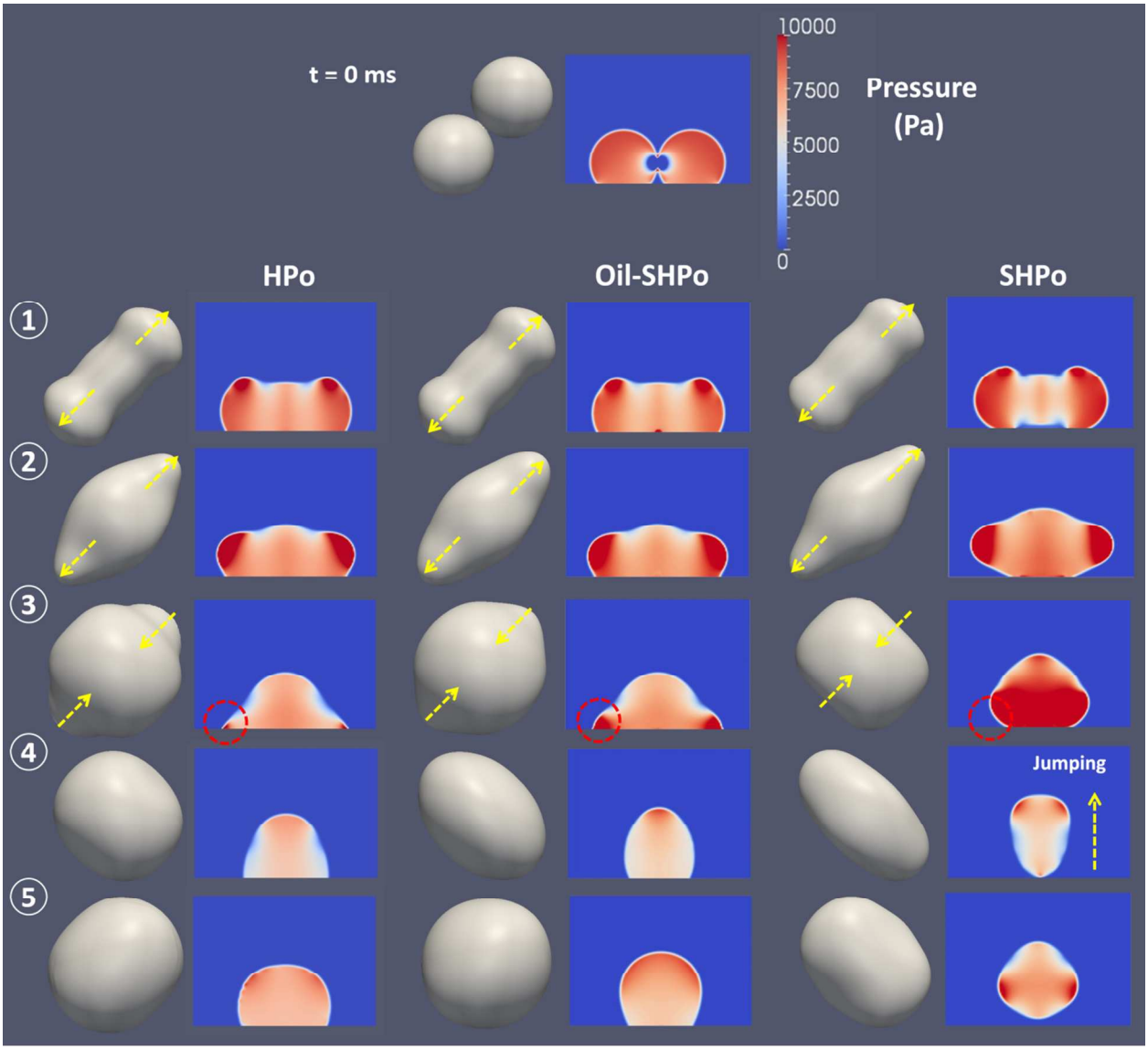

Figure 2: The time lapse images of the evolution of simulated droplets coalescing on SHPo, Oil-SHPo and HPo. The top views of the liquid-vapor interfacial areas are shown with the cross-sectional pressure distributions at point 1-5 representing t = 0.004, 0.007, 0.0108, 0.018, 0.024 (ms), respectively. The dotted circles in point 3 show the difference in the apparent receding angles and the resulting pressure field during the contact line receding on each surface.

Soft Matter Accepted Manuscript

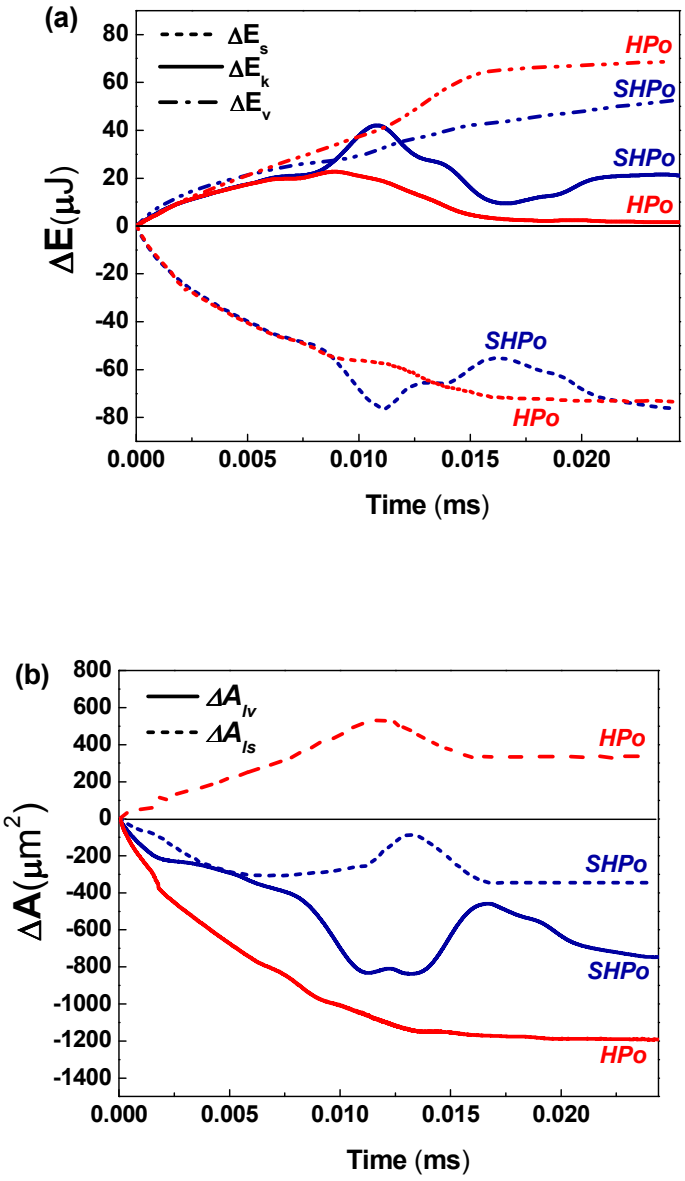

Figure 3: The changes in each energy term (a) and interfacial area (b) of droplets merged on HPo and SHPo as a function of time during the coalescence period.All the changes are calculated based on the initial state ($\Delta E = E - E_0$ and$\Delta A = A - A_0$). When the coalescence starts, the base area A_{ls} decreases on SHPo ($\Delta A_{ls} < 0$) while it increases on HPo ($\Delta A_{ls} > 0$), which makes SHPorelease large amount of surface energy even with relatively small decrease in the liquid-vapor area A_{lv}.

Soft Matter Accepted Manuscript

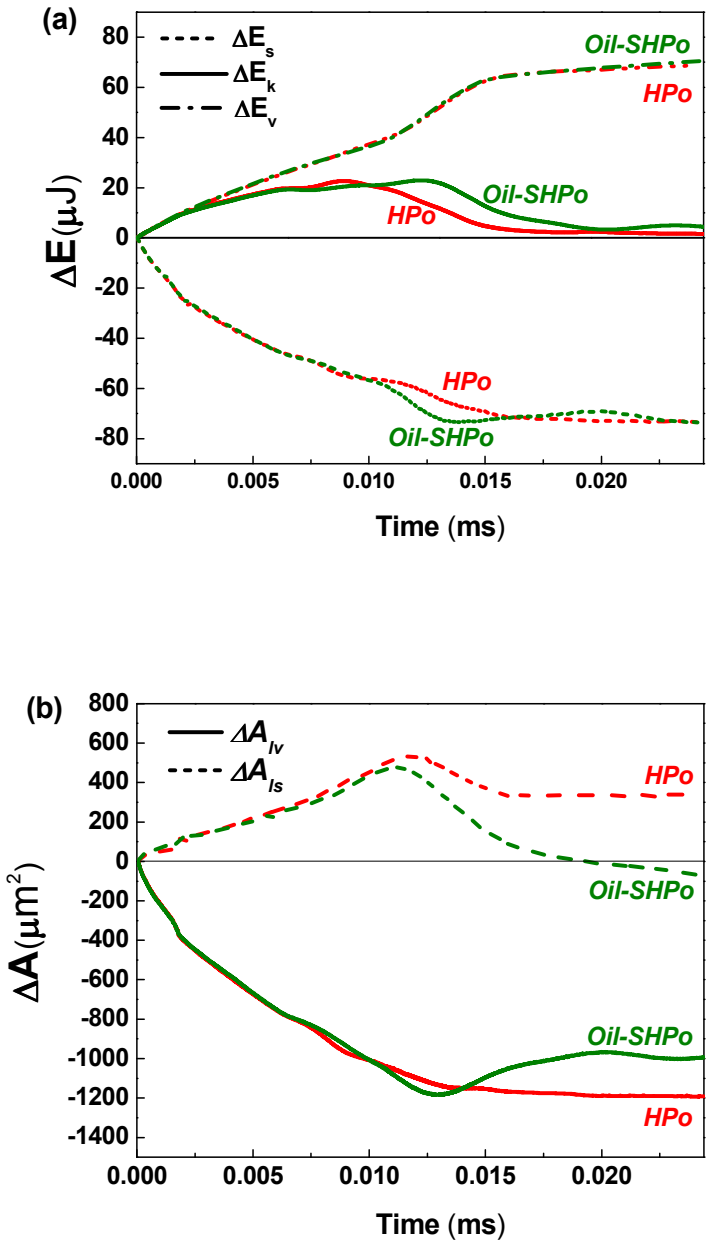

Figure 4: The changes in each energy term (a) and interfacial area (b) of droplets merged on HPo and Oil-SHPo as a function of time during the coalescence period.All the changes are calculated based on the initial state ($\Delta E = E - E_0$ and$\Delta A = A - A_0$). During the contact line receding, the base area decreases faster on Oil-SHPo due to the higher relaxation rate, which helps release larger amount of surface energy compared to HPo.

Soft Matter Accepted Manuscript